Stable Shaft-Sensorless Control of Permanent Magnet Synchronous Motors Using a Sliding Torque Observer*

Rong-Hwang HORNG** and Kan-Ping CHIN**

Two nonlinear sliding observers are developed for speed-sensorless control of permanent magnet synchronous motors. One of the observers estimates the rotor position and velocity based on the measurement of the motor current, while the other estimates load torque as well as rotor position and velocity. The lower bounds of the sliding gain, which guarantee the existence of the sliding manifold, and the upper bounds, which guarantee the stability of the digital implementation of the sliding observers, are also presented. Both theoretical analyses and experimental results demonstrate that, regardless of the observer used for speed-sensorless control, the steady-state velocity error converges even when an external load torque is applied to the rotor. However, when an external load is present, the position estimation error of the control system with torque estimation and compensation is significantly smaller than that of the system without torque estimation and compensation.

Key Words: Permanent Magnet Synchronous Motor, Shaft-Sensorless Control, Sliding Torque Observer, Stability Analysis

1. Introduction

Due to rapid progress in magnetic materials, power electronics, microprocessor technology and advanced control theory, ac permanent magnet synchronous motors (PMSM) have recently replaced dc motors as the new workhorse of industry. The speed of a synchronous motor is well known to be controllable in an open-loop simply by supplying phase voltages with an appropriate frequency. On the other hand, closed-loop servo control using position and velocity measurements has been widely adopted to enhance control precision, bandwidth and robustness. In a servo controlled motor, rotor position is usually measured with an encoder or a resolver, while rotor velocity is either measured with a tachometer or derived from position information. Since these shaft-mounted motion sensors are either fragile or bulky, and always expensive, it is desirable to replace these hardware sensors with software "state observers".

Early research on shaft-sensorless synchronous motor control typically estimated the rotor position by analyzing the current and voltage waveforms[1],[2]. However, this approach can only determine a few discrete angles and is not applicable to high-speed closed-loop control. Meanwhile, another research[3] developed rotor angle detection methods based on measuring back emf. However, these methods are inapplicable at low speeds and are sensitive to measurement noise. Recently, observer-based rotor position and velocity estimation methods have received considerable attention owing to their high accuracy and broad range of application. States such as the position and velocity of a motor are computed using a mathematical model of the motor and phase voltage and current measurements. Since all mathematical models are inevitably idealized and inaccurate, a compensation (innovation) term must be added to the observer to correct the observation error. Different observer theories essentially arise from different techniques of designing the innovation terms.

For speed sensorless synchronous motor control, Jones & Lang[4] and Low, Lee & Chang[5] developed observers based on Luenberger's theory[6]. Since the mathematical model of a PMSM is nonlinear, the observers based on the linear Luenberger's observer theory were only locally stable. Meanwhile, Cho, Hong, Oh & Youn[7] designed a sliding observer in a rotor reference frame using the theory proposed by

* Received 9th July, 2002 (No. 01-5082)

** Department of Mechanical Engineering, National Chiao-Tung University, 1001 Ta-Hsueh Road, Hsin-chu City, Taiwan, R.O.C. E-mail: rhhong@me.nctu.edu.tw

Walcott & Zak[8]. Since the transformation of phase currents from the fixed stator reference frame to the rotating rotor reference frame is position dependent, the overall stability of the observer is not guaranteed when the position is also obtained through observation. Furuhashi, Sangwongwanich & Okuma[9], Hsu[10] and Hu, Zhu, Li & Gao[11] developed nonlinear sliding observers in the stator reference frame based on Utkin's theory[12] of linear sliding observer design. The observer in Ref.(9) utilized only the equations of the electrical subsystem, and was unstable at low speed and high load torque. Meanwhile, full-order sliding observers were derived in Refs.(10) and (11). However, none of the above studies analyzed the ability of the observers to reject disturbance torque, which appears in almost all applications of the shaft-sensorless drives. Also, none of the above studies considered the stability of the closed-loop system and restriction of the innovation gain due to the digital implementation of the observer.

This study presents a different approach to position-and-velocity sensorless control of PMSM using a sliding observer. A torque estimation term is added to the observer in addition to the usual position and velocity estimation terms, and load torque is compensated according to the torque estimation. The sliding gain is well known to have to be lower-bounded to guarantee the existence of the sliding manifold and the stability of the sliding observer. However, during digital implementation, the sliding gain also needs to be upper-bounded to maintain the stability of the closed-loop system with the digital controller. This study also presents the upper bounds of the sliding observer obtained through discrete-time analysis of the linearized error dynamics of the closed-loop speed-sensorless control system.

2. Sliding Observer

It is well-known that sliding observers potentially offer advantages similar to those of sliding controllers, in particular inherent robustness of parametric uncertainty and easy application to important classes of nonlinear systems[8],[13]. Utkin proposed a sliding observer for linear systems in Ref.(12). A sliding observer for nonlinear systems can also be derived based on Utkin's approach:

Consider the following nonlinear system:

$$\frac{d\mathbf{x}}{dt}=\mathbf{f}(\mathbf{x},\mathbf{i},\mathbf{u},\mathbf{d})=\mathbf{f} \quad (1)$$

$$\frac{d\mathbf{i}}{dt}=\mathbf{g}(\mathbf{x},\mathbf{i},\mathbf{u},\mathbf{d})=\mathbf{g} \quad (2)$$

where $\mathbf{i}\in\mathbf{R}^n$ denotes the measurable states, $\mathbf{x}\in\mathbf{R}^m$ represents the states to be observed, $\mathbf{u}\in\mathbf{R}^p$ is the control input, and $\mathbf{d}\in\mathbf{R}^q$ denotes the disturbance input. If the sliding manifold is defined as:

$$\mathbf{S}=\hat{\mathbf{i}}-\mathbf{i}=\mathbf{0}$$

The following sliding observer is proposed for the system (1)-(2):

$$\dot{\hat{\mathbf{x}}}=\mathbf{f}(\hat{\mathbf{x}},\hat{\mathbf{i}},\mathbf{u})+\mathbf{G}\mathbf{w}=\hat{\mathbf{f}}+\mathbf{G}\mathbf{w} \quad (3)$$

$$\dot{\hat{\mathbf{i}}}=\mathbf{g}(\hat{\mathbf{x}},\hat{\mathbf{i}},\mathbf{u})-\mathbf{w}=\hat{\mathbf{g}}-\mathbf{w} \quad (4)$$

where

$$\mathbf{w}=K_s\cdot\mathrm{sgn}(\mathbf{S}),\ K_s>0$$

is the innovation term, K_s denotes the sliding gain; and $\mathbf{G}\in\mathbf{R}^{m\times n}$ represents the observer gain matrix. Subtracting (1)-(2) from (3)-(4) obtains the error dynamics of the observer:

$$\dot{\mathbf{e}}=\hat{\mathbf{f}}-\mathbf{f}+\mathbf{G}\mathbf{w} \quad (5)$$

$$\dot{\mathbf{S}}=\hat{\mathbf{g}}-\mathbf{g}-\mathbf{w} \quad (6)$$

where $\mathbf{e}=\hat{\mathbf{x}}-\mathbf{x}$ represents the error of the observed states. Suppose K_s is very large, then the stability of Eqs.(5)-(6) can be analyzed in a slow time-scale by letting

$$\delta=\frac{1}{K_s},\quad \tau=\frac{t}{\delta} \quad (7)$$

By substituting Eq.(7) into Eqs.(5) and (6), the error dynamics in the slow time-scale become

$$\frac{d\mathbf{e}}{d\tau}=\delta(\hat{\mathbf{f}}-\mathbf{f})+\mathbf{G}\,\mathrm{sgn}(\mathbf{S}) \quad (8)$$

$$\frac{d\mathbf{S}}{d\tau}=\delta(\hat{\mathbf{g}}-\mathbf{g})-\mathrm{sgn}(\mathbf{S}) \quad (9)$$

When $\delta\to 0$ (i.e. $K_s\to\infty$), Eqs.(8) and (9) become

$$\frac{d\mathbf{e}}{d\tau}=\mathbf{G}\,\mathrm{sgn}(\mathbf{S}) \quad (10)$$

$$\frac{d\mathbf{S}}{d\tau}=-\mathrm{sgn}(\mathbf{S}) \quad (11)$$

The stability of Eq.(11) can easily be shown by choosing a Lyapunov function

$$V=\frac{1}{2}\mathbf{S}^T\cdot\mathbf{S}.$$

The time derivative of V is

$$\dot{V}=\mathbf{S}^T\cdot\dot{\mathbf{S}}=-\mathbf{S}^T\cdot\mathrm{sgn}(\mathbf{S})=-|\mathbf{S}|<0,\ \forall\mathbf{S}\neq\mathbf{0} \quad (12)$$

Hence, when $\delta=0$, the observer states will reach the sliding manifold and all elements of $\mathbf{S}$ will converge to zero within a finite period. Since the solution of the differential Eq.(9) continuously depends on its parameters, all elements of $\mathbf{S}$ will converge to approximately zero when δ is sufficiently small (or K_s is sufficiently large). Moreover, K_s must at least satisfy

$$K_s>|\hat{\mathbf{g}}-\mathbf{g}| \quad (13)$$

to guarantee the stability of Eq.(9) and the existence of the sliding manifold. When the observer states reach the sliding manifold (i.e., $\mathbf{S}=0,\dot{\mathbf{S}}=0$), the equivalent value of the innovation term is derived from Eq.(6):

$$\mathbf{0}=\hat{\mathbf{g}}-\mathbf{g}-\mathbf{w}_{eq}\ \Rightarrow\ \mathbf{w}_{eq}=[\hat{\mathbf{g}}-\mathbf{g}]_{\mathbf{S}=\mathbf{0}} \quad (14)$$

To derive the error dynamics of the observer, Eq.(14) is substituted into Eq.(5)

$$\dot{\mathbf{e}}=[\hat{\mathbf{f}}-\mathbf{f}+\mathbf{G}(\hat{\mathbf{g}}-\mathbf{g})]_{\mathbf{S}=\mathbf{0}} \quad (15)$$

From Eq.(15), the stability and convergence rate of

the error of the observer states can be determined by choosing an appropriate observer gain **G**.

3. Observers for PMSM

The mathematical model of a smooth air-gap PMSM in the stator reference frame can be described by the following equations:

$$\frac{di_a}{dt}=-\frac{R}{L}i_a+\frac{KN}{L}\omega\sin(N\theta)+\frac{1}{L}v_a \tag{16}$$

$$\frac{di_b}{dt}=-\frac{R}{L}i_b-\frac{KN}{L}\omega\cos(N\theta)+\frac{1}{L}v_b \tag{17}$$

$$\dot{\theta}=\omega \tag{18}$$

$$\dot{\omega}=-\frac{KN}{H}(i_a\sin(N\theta)-i_b\cos(N\theta))-\frac{B}{H}\omega-\frac{\tau_L}{H} \tag{19}$$

where i_a and i_b denote the stator phase currents measured in the fixed a-b reference frame, v_a and v_b represent the command voltages measured in the a-b frame, H is the rotor inertia, R denotes the stator winding resistance, L represents the stator winding inductance, K is the motor constant, N denotes the number of magnetic pole pairs, and τ_L represents the external load torque.

3.1 Velocity observer

In Ref.(14), Wang analyzed the observability of a nonlinear PMSM model (16) - (19) with phase currents as outputs and phase voltages as inputs using the Lie derivative method[15] and the result showed that the nonlinear system is always observable except at $\omega=0$, where the rank of the observability matrix is not full but equal to 4. This fact makes the observer gains go to infinity when $\omega=0$ as will be discussed later.

According to the procedure outlined above, the sliding manifold and corresponding innovation terms must first be defined as

$$\mathbf{S}=\begin{Bmatrix}S_a\\S_b\end{Bmatrix}=\begin{Bmatrix}\hat{i}_a-i_a\\\hat{i}_b-i_b\end{Bmatrix}=\mathbf{0};\quad \mathbf{w}=\begin{Bmatrix}w_a\\w_b\end{Bmatrix}=\begin{Bmatrix}K_s\,\mathrm{sgn}(S_a)\\K_s\,\mathrm{sgn}(S_b)\end{Bmatrix}$$

The sliding observer is constructed as follows:

$$\dot{\hat{i}}_a=-\frac{R}{L}\hat{i}_a+\frac{KN}{L}\hat{\omega}\sin(N\hat{\theta})+\frac{1}{L}v_a-w_a \tag{20}$$

$$\dot{\hat{i}}_b=-\frac{R}{L}\hat{i}_b-\frac{KN}{L}\hat{\omega}\cos(N\hat{\theta})+\frac{1}{L}v_b-w_b \tag{21}$$

$$\dot{\hat{\theta}}=\hat{\omega} \tag{22}$$

$$\dot{\hat{\omega}}=-\frac{KN}{H}(\hat{i}_a\sin(N\hat{\theta})-\hat{i}_b\cos(N\hat{\theta}))-\frac{B}{H}\hat{\omega}+G_1w_a+G_2w_b \tag{23}$$

where G_1 and G_2 denote the observer gains. The error dynamics of the observer are obtained by subtracting (16) - (19) from (20) - (23):

$$\dot{S}_a=-\frac{R}{L}S_a+\frac{KN}{L}(\hat{\omega}\sin(N\hat{\theta})-\omega\sin(N\theta))-w_a \tag{24}$$

$$\dot{S}_b=-\frac{R}{L}S_b-\frac{KN}{L}(\hat{\omega}\cos(N\hat{\theta})-\omega\cos(N\theta))-w_b \tag{25}$$

$$\dot{e}_\theta=e_\omega \tag{26}$$

$$\dot{e}_\omega=-\frac{KN}{H}(\hat{i}_a\sin(N\hat{\theta})-i_a\sin(N\theta)-\hat{i}_b\cos(N\hat{\theta})+i_b\cos(N\theta))-\frac{B}{H}e_\omega+G_1w_a+G_2w_b+\frac{\tau_L}{H} \tag{27}$$

Let

$$K_{s,\min}=\max\left\{\left|\frac{KN}{L}(\hat{\omega}\sin(N\hat{\theta})-\omega\sin(N\theta))\right|,\left|\frac{KN}{L}(\hat{\omega}\cos(N\hat{\theta})-\omega\cos(N\theta))\right|\right\}, \tag{28}$$

the observer states will reach the sliding manifold, i.e., $\mathbf{S}=\mathbf{0}$ and $\dot{\mathbf{S}}=\mathbf{0}$ for $K_s>K_{s,\min}$. Under the circumstances, the equivalent value of the innovation terms becomes

$$w_a=\frac{KN}{L}(\hat{\omega}\sin(N\hat{\theta})-\omega\sin(N\theta)) \tag{29}$$

$$w_b=-\frac{KN}{L}(\hat{\omega}\cos(N\hat{\theta})-\omega\cos(N\theta)) \tag{30}$$

To determine the gains G_1 and G_2, Eqs.(29), (30) must first be substituted into Eq.(27) to obtain the error dynamics of the states requiring observation. The error dynamics are then linearized around the observer states, $\hat{\theta}$ and $\hat{\omega}$:

$$\dot{e}_\omega=-\left\{\frac{B}{H}-\frac{KN}{L}(G_i\sin(N\hat{\theta})-G_2\cos(N\hat{\theta}))\right\}e_\omega+KN^2\left\{\frac{\hat{\omega}}{L}(G_1\cos(N\hat{\theta})+G_2\sin(N\hat{\theta}))-\frac{1}{H}(\hat{i}_a\cos(N\hat{\theta})+\hat{i}_b\sin(N\hat{\theta}))\right\}e_\theta+\frac{\tau_L}{H} \tag{31}$$

If the eigenvalues of Eq.(31) are both chosen as negative real numbers, $-\lambda_\theta$ and $-\lambda_\omega$, then Eq.(31) becomes

$$\dot{e}_\omega+(\lambda_\theta+\lambda_\omega)e_\omega+\lambda_\theta\lambda_\omega e_\theta=\frac{\tau_L}{H} \tag{32}$$

The observer gains G_1 and G_2 are determined by solving Eqs.(31) and (32):

$$\begin{Bmatrix}G_1\\G_2\end{Bmatrix}=\begin{bmatrix}\cos(N\hat{\theta}) & N\hat{\omega}\sin(N\hat{\theta})\\\sin(N\hat{\theta}) & -N\hat{\omega}\cos(N\hat{\theta})\end{bmatrix}\times\begin{Bmatrix}\frac{L}{H\hat{\omega}}(\hat{i}_a\cos(N\hat{\theta})+\hat{i}_b\sin(N\hat{\theta}))-\frac{L\lambda_\theta\lambda_\omega}{KN^2\hat{\omega}}\\\frac{L}{KN^2\hat{\omega}}\left(\frac{B}{H}-(\lambda_\theta+\lambda_\omega)\right)\end{Bmatrix}.$$

Noted that $\hat{\omega}$ is in the denominators of the equations when calculating the observer gains, G_1 and G_2 by the fact that the system is unobservable at $\omega=0$.

From Eq.(32), when $K_s\to\infty$, the position and the velocity estimation errors will both converge to zero if the system contains no load torque. On the other hand, if the load torque is a constant, then the velocity error still converges to zero, while the steady-state position error remains constant:

$$e_\theta=-\frac{\tau_L}{H\lambda_\theta\lambda_\omega}$$

The magnitude of the position estimation error can be reduced by increasing λ_θ, λ_ω and K_s. For the further

reduction of the position estimation error, a torque observer is presented below.

3.2 Torque observer

In Ref.(14), Wang obtained the same result as discussed in the previous section when the PMSM model (16) - (19) is augmented with the fifth equation:

$$\dot{\tau}_L = M\cos(N\theta+\phi) \tag{33}$$

where M and ϕ are any constants. Theoretically, the observer can be designed to remain stable under both constant torque and periodically varying torque. Hence, position, velocity and periodically varying load torque can all be observed. In practice, provided the period of the load torque variation significantly exceeds the sampling period of the observer, the load torque can be considered to be a constant during a given sample period. Consequently, by letting $M=\phi=0$ in Eq.(33) the sliding observer (20) - (23) can be augmented with a constant torque observer

$$\dot{\hat{\tau}}_L = G_3 w_a + G_4 w_b \tag{34}$$

where G_3 and G_4 are observer gains. Since load torque τ_L is considered to be a state in this case, Eqs.(23) and (27) must also be changed into Eqs.(35) and (36) respectively:

$$\dot{\hat{\omega}} = -\frac{KN}{H}\hat{i}_a\sin(N\hat{\theta}) + \frac{KN}{H}\hat{i}_b\cos(N\hat{\theta}) - \frac{B}{H}\hat{\omega} - \frac{1}{H}\hat{\tau}_L + G_1 w_a + G_2 w_b \tag{35}$$

$$\dot{e}_\omega = -\frac{KN}{H}(\hat{i}_a\sin(N\hat{\theta}) - i_a\sin(N\theta) - \hat{i}_b\cos(N\hat{\theta}) + i_b\cos(N\theta)) - \frac{B}{H}e_\omega + G_1 w_a + G_2 w_b + \frac{e_\tau}{H} \tag{36}$$

Subtracting (33) from Eq.(34) obtains the error dynamics of the fifth term:

$$\dot{e}_\tau = G_3 w_a + G_4 w_b \tag{37}$$

Under such conditions, the linearized error dynamics at $\mathbf{S}=\mathbf{0}$ and $\dot{\mathbf{S}}=\mathbf{0}$ become

$$\begin{Bmatrix}\dot{e}_\omega\\ \dot{e}_\theta\\ \dot{e}_\tau\end{Bmatrix} = \begin{bmatrix}a_1 & a_2 & -\frac{1}{H}\\ 1 & 0 & 0\\ a_3 & a_4 & 0\end{bmatrix}\begin{Bmatrix}e_\omega\\ e_\theta\\ e_\tau\end{Bmatrix} \tag{38}$$

where $e_\tau = \hat{\tau}_L - \tau_L$,

$$a_1 = -\frac{B}{H} + \frac{KN}{L}(G_1\sin(N\hat{\theta}) - G_2\cos(N\hat{\theta})),$$

$$a_2 = KN^2\left\{\frac{\hat{\omega}}{L}(G_1\cos(N\hat{\theta}) + G_2\sin(N\hat{\theta})) - \frac{1}{H}(\hat{i}_a\cos(N\hat{\theta}) + \hat{i}_b\sin(N\hat{\theta}))\right\},$$

$$a_3 = \frac{KN}{L}(G_3\sin(N\hat{\theta}) - G_4\cos(N\hat{\theta})),$$

$$a_4 = \frac{KN^2}{L}\hat{\omega}(G_3\cos(N\hat{\theta}) + G_4\sin(N\hat{\theta})).$$

By setting the eigenvalues as $-\lambda_\theta$, $-\lambda_\omega$, and $-\lambda_\tau$, the observer gains are solved as:

$$\begin{Bmatrix}G_1\\ G_2\end{Bmatrix} = \begin{bmatrix}\cos(N\hat{\theta}) & N\hat{\omega}\sin(N\hat{\theta})\\ \sin(N\hat{\theta}) & -N\hat{\omega}\cos(N\hat{\theta})\end{bmatrix} \times \begin{Bmatrix}\frac{L}{H\hat{\omega}}(\hat{i}_a\cos(N\hat{\theta}) + \hat{i}_b\sin(N\hat{\theta})) - \frac{L\lambda_3}{KN^2\hat{\omega}}\\ \frac{L}{KN^2\hat{\omega}}\left(\frac{B}{H} - \lambda_4\right)\end{Bmatrix}$$

$$\begin{Bmatrix}G_3\\ G_4\end{Bmatrix} = \frac{HL\lambda_\theta\lambda_\omega\lambda_\tau}{KN^2\hat{\omega}}\begin{Bmatrix}\sin(N\hat{\theta}) + \cos(N\hat{\theta})\\ \sin(N\hat{\theta}) - \cos(N\hat{\theta})\end{Bmatrix}$$

where $\lambda_3 = \lambda_\theta\lambda_\omega + \lambda_\omega\lambda_\tau + \lambda_\tau\lambda_\theta - \frac{\lambda_\theta\lambda_\omega\lambda_\tau}{N\hat{\omega}}$, and $\lambda_4 = \lambda_\theta + \lambda_\omega + \lambda_\tau$. Since the system is unobservable at $\omega=0$, the observer gains, G_1, G_2, G_3, and G_4, become infinite as the rotating speed, ω, is approaching to zero.

Since the eigenvalues of the error dynamics are three negative real numbers, the position, velocity and load torque estimation errors all asymptotically converge to zero when $K_s\to\infty$. However, since K_s is a large finite number, both the position and load torque estimation errors converge to small non-zero numbers, while the velocity estimation error converges to zero.

4. Stability Analysis

This section discusses the local stability of the linearized error dynamics of the digital implementation of the speed-sensorless control system except at $\omega=0$, where the system is unobservable. Since the velocity observer is only a special case of the torque observer where λ_τ equals zero, only the stability of the closed-loop speed-sensorless control system based on the torque observer needs to be discussed.

To ensure local stability at each velocity, the following procedure is conducted:

1) Substitute the observer gains, G_1, G_2, G_3, and G_4 into Eqs.(24) - (26), (36) and (37).

2) Replace the estimated states, $\hat{i}_a$, $\hat{i}_b$, $\hat{\theta}$, $\hat{\omega}$, and $\hat{\tau}$ by S_a+i_a, S_b+i_b, $e_\theta+\theta$, $e_\omega+\omega$, and $e_\tau+\tau$ respectively.

3) Change the innovation terms, w_a and w_b, and limit the range of S_a and S_b:

The innovation terms, w_a and w_b, are discontinuous around $S_a=0$ and $S_b=0$. For analytical simplicity, w_a and w_b are replaced by $K_s\,\mathrm{sat}(S_a,\varepsilon)$ and $K_s\,\mathrm{sat}(S_b,\varepsilon)$ respectively, where $\varepsilon>0$ and the function $K_s\,\mathrm{sat}(S_a,\varepsilon)$ is as displayed in Fig. 1. Additionally,

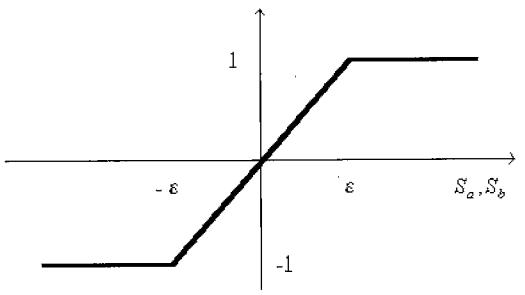

Fig. 1 Function sat(S,ε)

the innovation terms are assumed to force the observer states into a close vicinity of the sliding manifold. As a result, stability analysis is only required for the small region where $|S_a| \leq \varepsilon$ and $|S_b| \leq \varepsilon$. In this region, nonlinear innovation terms can be replaced by linear terms, $\frac{K_s}{\varepsilon}S_a$ and $\frac{K_s}{\varepsilon}S_b$. Furthermore, Eqs.(24) - (26), (36) and (37) can be rewritten as Eqs.(39) - (43).

$$\dot{S}_a = \frac{KN^2\omega\cos(N\theta)}{L}e_\theta + \frac{KN\sin(N\theta)}{L}e_\omega - \left(\frac{R}{L}+\frac{K_s}{\varepsilon}\right)S_a \tag{39}$$

$$\dot{S}_b = \frac{KN^2\omega\sin(N\theta)}{L}e_\theta - \frac{KN\cos(N\theta)}{L}e_\omega - \left(\frac{R}{L}+\frac{K_s}{\varepsilon}\right)S_b \tag{40}$$

$$\dot{e}_\theta = e_\omega \tag{41}$$

$$\begin{aligned}\dot{e}_\omega = &-\frac{1}{H}(e_\tau + Be_\omega + KN^2e_\theta(i_a\cos(N\theta)+i_b\sin(N\theta)) + KNS_a\sin(N\theta) - KNS_b\cos(N\theta))\\ &+\frac{LK_s(B-HK_1)(S_a\sin(N(\theta+e_\theta))-S_b\cos(N(\theta+e_\theta)))}{HKN\varepsilon}\\ &+\frac{LK_s(S_a\cos(N(\theta+e_\theta))+S_b\sin(N(\theta+e_\theta)))(i_a\cos(N(\theta+e_\theta))+i_b\sin(N(\theta+e_\theta)))}{H\varepsilon(\omega+e_\omega)}\\ &+\frac{LK_s(K_3-NK_2)(S_a\cos(N(\theta+e_\theta))+S_b\sin(N(\theta+e_\theta)))}{HN^2\varepsilon(\omega+e_\omega)}\\ &+\frac{LK_s(S_a\cos(N(\theta+e_\theta))+S_b\sin(N(\theta+e_\theta)))^2}{H\varepsilon(\omega+e_\omega)}\end{aligned} \tag{42}$$

$$\begin{aligned}\dot{e}_\tau = &\frac{HLK_3K_s}{KN^2\varepsilon(\omega+e_\omega)}\{\cos[N(\theta+e_\theta)](S_a-S_b)\\ &+\sin[N(\theta+e_\theta)](S_a+S_b)\}\end{aligned} \tag{43}$$

where $K_1=\lambda_\theta+\lambda_\omega+\lambda_\tau$, $K_2=\lambda_\theta\lambda_\omega+\lambda_\omega\lambda_\tau+\lambda_\theta\lambda_\tau$, and $K_3=\lambda_\theta\lambda_\omega\lambda_\tau$.

4) Calculate the equilibrium point:

Two sets of equilibrium points are found by letting (39) - (43) equal zero. One of the equilibrium points is located at $S_a=0$, $S_b=0$, $e_\omega=0$, $e_\tau=0$ and $e_\theta=\frac{2M\pi}{N}$, where $M\in\mathbf{Z}$. Meanwhile, the other one is at

$$S_a = -\frac{KN\varepsilon\omega(\cos(N\theta)+\sin(N\theta))}{R\varepsilon+LK_s}, \tag{44}$$

$$S_b = \frac{KN\varepsilon\omega(\cos(N\theta)-\sin(N\theta))}{R\varepsilon+LK_s} \tag{45}$$

$$e_\omega = 0$$

$$e_\theta = -\frac{(4M+1)\pi}{2N}$$

$$e_\tau = \frac{1}{(R\varepsilon+LK_s)^2}\begin{pmatrix} KNR\varepsilon^2(-KN\omega+Ri_a\cos(N\theta)+Ri_a\sin(N\theta)-Ri_b\cos(N\theta)+Ri_b\sin(N\theta))\\ +KLNR\varepsilon K_s(2i_a\cos(N\theta)+i_a\sin(N\theta)+2i_b\sin(N\theta)-i_b\cos(N\theta))\\ +LR\varepsilon K_s\left(B\omega-H\omega K_1+\frac{HK_2}{N}-\frac{HK_3}{N^2\omega}\right)\\ +L^2K_s^2\left(B\omega+KNi_a\cos(N\theta)+KNi_b\sin(N\theta)-H\omega K_1+\frac{HK_2}{N}-\frac{HK_3}{N^2\omega}\right)\end{pmatrix}.$$

From the above equations, the second equilibrium is a function of the angular position and changes accordingly. Additionally, from Eqs.(44) and (45), the maximum value of S_a and S_b is bounded by $\frac{\sqrt{2}KN\varepsilon\omega}{R\varepsilon+LK_s}$ at the second equilibrium point. Given this bound, and assuming that $|S_a|\leq\varepsilon$ and $|S_b|\leq\varepsilon$, it is concluded that the second equilibrium exists only when $K_s>(K_{s,\max})_{E2}=(\sqrt{2}KN\omega-R\varepsilon)/L$.

5) Derive the linearized error dynamics around each equilibrium point:

A set of equations describing the linearized error dynamics can be derived by linearizing (39) - (43) around the first equilibrium point:

$$\dot{S}_a = -\left(\frac{R}{L}+\frac{K_s}{\varepsilon}\right)S_a + \frac{KN}{L}(N\omega\cos(N\theta)e_\theta+\sin(N\theta)e_\omega) \tag{46}$$

$$\dot{S}_b = -\left(\frac{R}{L}+\frac{K_s}{\varepsilon}\right)S_b + \frac{KN}{L}(N\omega\sin(N\theta)e_\theta-\cos(N\theta)e_\omega) \tag{47}$$

$$\dot{e}_\theta = e_\omega \tag{48}$$

$$\dot{e}_\omega=\left(\begin{array}{l}-\frac{KN}{H}\sin(N\theta)+\frac{K_sL\sin(N\theta)}{KN\varepsilon}\left(\frac{B}{H}-K_1\right)\\+\frac{K_sL\cos(N\theta)}{H\varepsilon\omega}(i_a\cos(N\theta)+i_b\sin(N\theta))\\+\frac{K_sL\cos(N\theta)}{KN^2\varepsilon\omega}\left(-K_2+\frac{K_3}{N\omega}\right)\end{array}\right)S_a+\left(\begin{array}{l}\frac{KN}{H}\cos(N\theta)+\frac{K_sL\cos(N\theta)}{KN\varepsilon}\left(-\frac{B}{H}+K_1\right)\\+\frac{K_sL\sin(N\theta)}{H\varepsilon\omega}(i_a\cos(N\theta)+i_b\sin(N\theta))\\+\frac{K_sL\sin(N\theta)}{KN^2\varepsilon\omega}\left(-K_2+\frac{K_3}{N\omega}\right)\end{array}\right)S_b$$
$$+\left(-\frac{KN^2}{H}i_a\cos(N\theta)-\frac{KN^2}{H}i_b\sin(N\theta)\right)e_\theta-\frac{B}{H}e_\omega-\frac{1}{H}e_\tau \tag{49}$$

$$\dot{e}_\tau=\frac{K_3K_sHL}{KN^2\varepsilon\omega}(\cos(N\theta)+\sin(N\theta))S_a+\frac{K_3K_sHL}{KN^2\varepsilon\omega}(-\cos(N\theta)+\sin(N\theta))S_b \tag{50}$$

Similarly, around the second equilibrium point, the linearized error dynamics can be derived as follows:

$$\dot{S}_a=-\left(\frac{R}{L}+\frac{K_s}{\varepsilon}\right)S_a+\frac{KN^2}{L}\omega\cos\left(N\theta-\frac{\pi}{2}+2M\pi\right)e_\theta+\frac{KN}{L}\sin\left(N\theta-\frac{\pi}{2}+2M\pi\right)e_\omega \tag{51}$$

$$\dot{S}_b=-\left(\frac{R}{L}+\frac{K_s}{\varepsilon}\right)S_b+\frac{KN^2}{L}\omega\sin\left(N\theta-\frac{\pi}{2}+2M\pi\right)e_\theta-\frac{KN}{L}\cos\left(N\theta-\frac{\pi}{2}+2M\pi\right)e_\omega \tag{52}$$

$$\dot{e}_\theta=e_\omega \tag{53}$$

$$\dot{e}_\omega=\frac{1}{R\varepsilon+LK_s}\left(\begin{array}{l}\frac{KNR\varepsilon}{H}\cos(N\theta)+K_sL\cos(N\theta)\left(\frac{KN}{H}-\frac{BR}{HKN}+\frac{RK_1}{KN}\right)\\+K_sL\sin(N\theta)\left(-\frac{2KN}{H}-\frac{RK_2}{KN^2\omega}+\frac{RK_3}{KN^3\omega^2}\right)\\+\frac{K_sL}{H\omega}\left(i_a\sin^2(N\theta)-\frac{i_b\sin(2N\theta)}{2}\right)\left(R+\frac{K_sL}{\varepsilon}\right)\\+\frac{K_s^2L^2\cos(N\theta)}{KN\varepsilon}\left(-\frac{B}{H}+K_1\right)+\frac{K_s^2L^2\sin(N\theta)}{KN^2\varepsilon\omega}\left(-K_2+\frac{K_3}{N\omega}\right)\end{array}\right)S_a$$
$$+\frac{1}{R\varepsilon+LK_s}\left(\begin{array}{l}\frac{KNR\varepsilon}{H}\sin(N\theta)+K_sL\sin(N\theta)\left(\frac{KN}{H}-\frac{BR}{HKN}+\frac{RK_1}{KN}\right)\\+K_sL\cos(N\theta)\left(\frac{2KN}{H}+\frac{RK_2}{KN^2\omega}-\frac{RK_3}{KN^3\omega^2}\right)\\+\frac{K_sL}{2H\omega}\left(-i_a\sin(2N\theta)+i_b+i_b\cos(2N\theta)\right)\left(R+\frac{K_sL}{\varepsilon}\right)\\+\frac{K_s^2L^2\sin(N\theta)}{KN\varepsilon}\left(-\frac{B}{H}+K_1\right)+\frac{K_s^2L^2\cos(N\theta)}{KN^2\varepsilon\omega}\left(K_2-\frac{K_3}{N\omega}\right)\end{array}\right)S_b$$
$$+\frac{1}{(R\varepsilon+LK_s)^2}\left(\begin{array}{l}\frac{-BR^2\varepsilon^2-K^2LN^2\varepsilon K_s-2BLR\varepsilon K_s-BL^2K_s^2}{H}\\+LR\varepsilon K_s\left(\frac{KNi_a\sin(N\theta)-KNi_b\cos(N\theta)}{H\omega}-\frac{K_2}{N\omega}+\frac{2K_3}{N^2\omega^2}\right)\\+L^2K_s^2\left(\frac{KNi_a\sin(N\theta)-KNi_b\cos(N\theta)}{H\omega}-\frac{K_2}{N\omega}+\frac{2K_3}{N^2\omega^2}\right)\end{array}\right)e_\omega-\frac{1}{H}e_\tau \tag{54}$$

$$\dot{e}_\tau=\frac{K_3K_sHL}{KN^2\varepsilon\omega}(-\cos(N\theta)+\sin(N\theta))S_a+\frac{K_3K_sHL}{KN^2\varepsilon\omega}(-\cos(N\theta)-\sin(N\theta))S_b-\frac{2HLK_3K_s}{R\varepsilon+LK_s} \tag{55}$$

6) Compute the states of the PMSM:

The states of the PMSM can be derived from the mathematical model of the PMSM in the rotor reference frame[14], as shown below:

$$\frac{di_d}{dt}=-\frac{R}{L}i_d+Ni_q\omega+\frac{1}{L}v_d \tag{56}$$

$$\frac{di_q}{dt}=-\frac{R}{L}i_q-\frac{KN}{L}\omega-Ni_d\omega+\frac{1}{L}v_q \tag{57}$$

$$\frac{d\theta}{dt}=\omega \tag{58}$$

$$\frac{d\omega}{dt}=\frac{KN}{H}i_q-\frac{B}{H}\omega \tag{59}$$

where i_d and i_q denote the stator phase currents measured in the rotor reference frame, while v_d and v_q represent the command voltages measured in the rotor reference frame.

Let $\omega=$constant$\neq0$ and $i_d=0$, θ and i_q can be derived from Eqs. (58) and (59). Meanwhile, i_a and i_b can be derived by transforming i_d and i_q into the stator reference frame. Consequently, the states of PMSM can be described by

$$\omega=\text{constant}\neq0$$
$$\theta=\theta_0+\omega\cdot t$$
$$i_d=0$$
$$i_q=\frac{B\omega+\tau_L}{KN}$$
$$\left\{\begin{array}{l}i_a\\i_b\end{array}\right\}=\left[\begin{array}{ll}\cos(N\theta) & -\sin(N\theta)\\\sin(N\theta) & \cos(N\theta)\end{array}\right]\left\{\begin{array}{l}i_d\\i_q\end{array}\right\}=\left\{\begin{array}{l}-i_q\sin(N\theta)\\i_q\cos(N\theta)\end{array}\right\}$$

7) Plot the root loci of the linearized error dynamics, and analyze the stability of the closed-loop system:

By substituting the states of the PMSM and the observer gains into Eqs. (46) - (50) and (51) - (55), the roots of the error dynamics can be calculated and

plotted. In Section 3, the desired eigenvalues, λ_θ, λ_ω, λ_τ, of the observer error dynamics on the sliding manifold are specified first, and then the observer gain matrix, **G**, is calculated from these eigenvalues. Consequently, the observer gains are determined from the desired observer behavior. On the other hand, the sliding gain, K_s, was only required to satisfy Eqs. (13), (28), or to be "large enough" to guarantee the existence of the sliding manifold. However, during digital implementation, a computer carries out the computation required by the observer and control laws. Under such circumstances, K_s not only needs to be lower-bounded, but also upper-bounded to maintain the stability of the discrete-time system. Hence, the range of the sliding gain must be identified to permit stable digital implementation.

The Delta Transformation method[16] is used to analyze the stability at the discrete time, since this method requires minimal modification to transform a continuous-time model to its discrete-time equivalent. For instance, the discrete-time models of the continuous-time error dynamics (46) - (50) and (51) - (55) can easily be obtained by turning all the time-derivative terms into difference terms:

$$\dot{S}_a \rightarrow \frac{\Delta S_a}{T}$$

$$\dot{S}_b \rightarrow \frac{\Delta S_b}{T}$$

$$\dot{e}_\theta \rightarrow \frac{\Delta e_\theta}{T}$$

$$\dot{e}_\omega \rightarrow \frac{\Delta e_\omega}{T}$$

$$\dot{e}_\tau \rightarrow \frac{\Delta e_\tau}{T}$$

where T denotes the sample period. Under such conditions, the eigenvalues of the discrete-time model is exactly same as those of the continuous-time model. The continuous-time system is well known to be asymptotically stable if and only if all the eigenvalues of the continuous-time system satisfy $\mathrm{Re}\{p_i\}<0$, where $\mathrm{Re}\{p_i\}$ denotes the real part of the eigenvalue, p_i. However, according to the Delta transformation theory, for example in Ref. (16), the discrete-time system is stable if and only if the eigenvalues of the discrete-time system satisfy $\frac{T}{2}|p_i|^2 + \mathrm{Re}\{p_i\}<0$. In the pole plane, the stability boundary of the discrete-time system can be represented as a circle with a radius that is inversely proportional to the sample period T, at the left-half plane. The following are the main differences between a discrete-time system and a continuous-time system:

a) The range of eigenvalues for a stable discrete-time system is always smaller than that for a stable continuous-time system;

b) The magnitude of the eigenvalues for a stable discrete-time system is always upper-bounded;

c) The higher the sample frequency in a discrete-time system, the larger the stability range;

d) A continuous-time system is equivalent to a discrete-time system with infinite sample frequency.

For example, given the motor parameters listed in Table 1, the observer gains $\lambda_\theta=10$ Hz, $\lambda_\omega=60$ Hz, $\lambda_\tau=2$ Hz, and the operation conditions $\omega=1\,000$ rpm, $\tau_L=0$ N·m, and $\varepsilon=1$, then the root loci of the first equilibrium point from Eqs. (46) - (50) when K_s varies from 0 to 8 000 are shown in Fig. 2. Similarly, the root loci of the second equilibrium point computed from Eqs. (51) - (55) are illustrated in Fig. 3.

Table 1 Parameters of the Sinano #7CB30-2SE6F motor

No. of pole-pair	N = 4
Resistance	R = 2.5 Ω
Inductance	L = 5.97×10^{-3} H
Motor Constant	K = 5.795×10^{-2} V·S/rad
Rotor inertia	H = 6.45×10^{-5} kg·m^2
Viscous Coeffi.	B = 8.06×10^{-5} N·m·s/rad

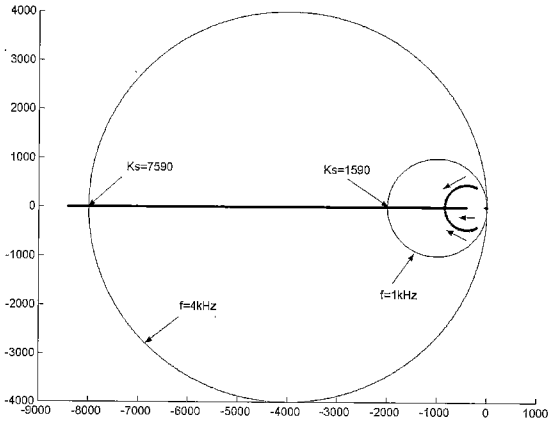

Fig. 2 Root loci of the error dynamics around the first equilibrium points

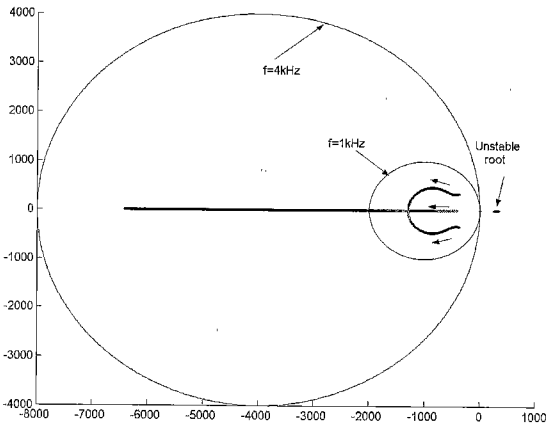

Fig. 3 Root loci of the error dynamics around the second equilibrium points

Consider the root loci of the first equilibrium point in Fig. 2. The large circle represents the stability boundary when the sample frequency is 4 kHz, while the small circle represents the stability boundary when the sample frequency is 1 kHz. From Fig. 2, the discrete-time system is locally stable if the sample rate is 4 kHz and K_s is smaller than 7 590, or if the sample rate is 1 kHz and K_s is smaller than 1 590. Therefore, an upper bound, $(K_{s,\max})_T$, exists for each sample rate (or sample period). Additionally, the higher the sample rate, the larger $(K_{s,\max})_T$.

Consider the root loci of the second equilibrium point in Fig. 3. An unstable pole exists on the right-half plane. Consequently, the system is unstable regardless of the sample rate. From the analyses above, an upper bound, $K_s \leq (K_{s,\max})_{E2} = (\sqrt{2}KN\omega - R\varepsilon)/L$, can be chosen to prevent the appearance of the second equilibrium point.

In conclusion, K_s should be bounded by the following rules to ensure system stability:

- From Eqs. (13) and (28), K_s must be larger than the lower bound, $K_{s,\min}$, to guarantee the stability of Eq. (9) and the existence of the sliding manifold.
- To ensure the stability of the first equilibrium point, an upper bound, $K_s \leq (K_{s,\max})_T$, should be calculated for each velocity ω and sample rate.
- To prevent a second, always unstable, equilibrium point from appearing, another upper bound, $K_s \leq (K_{s,\max})_{E2} = (\sqrt{2}KN\omega - R\varepsilon)/L$, should also be imposed on the range of K_s.

5. Experiments

The experimental setup includes a Sinano #7CB30-2SE6F permanent magnet synchronous motor (whose parameters are listed in Table 1), the power stage of a Micro Trend UT90 driver, a control card made in house, and a 586 PC. The control card is intended to convert the analog phase current measurements into digital signals, decode the encoder signals and the Hall-effect sensor signals, and generate space vector pulse width modulation (SVPWM) switching signals to control the power stage. Meanwhile, the 586 PC is used to compute the control algorithms and the coordinate transformations for the vector space between stator reference frame and rotor reference frame.

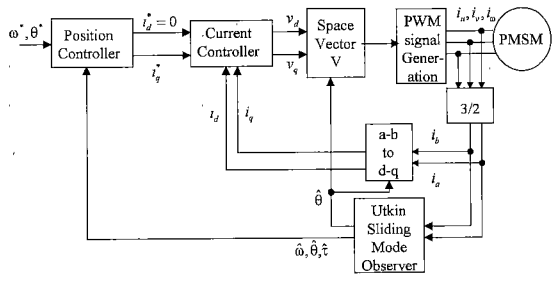

Fig. 4 Block diagram of the shaft-sensorless speed controller

Experiments involving closed-loop shaft-sensorless speed control are performed using both the velocity observer, Eqs. (20) - (23) and torque observer, Eqs. (20) - (22), (34), (35). Figure 4 displays the block diagram of the control system. The control algorithm used in the experiments is the two-loop controller developed in Ref. (14). Since a nonlinear PMSM model (16) - (19), (33) is unobservable at $\omega=0$ with phase currents as outputs and phase voltages as inputs, both observers can't estimate the states of motor at $\omega=0$. In our implementation of observer, a small value $\bar{\omega}_{low}=1$ rad/s is used instead of $\bar{\omega}$ when $0 \leq |\bar{\omega}| \leq \bar{\omega}_{low}$ to obtain observer gains and this will make the performance not effective at low speeds ($\omega \cong 0$). During the experiments, the position, velocity, and torque feedback used in the speed controller are calculated from the observers, and the encoder is only used to measure the motor velocity and position to verify the effectiveness of the observers. The sample rates for the velocity controller and the current controller are 1 kHz and 4 kHz, respectively, while the bandwidth of the velocity controller and the current controller are set at 20 Hz and 300 Hz, respectively. Additionally, the velocity observer gains are $\lambda_\theta=10$ Hz, $\lambda_\omega=60$ Hz, $\varepsilon=1$ and $K_s=30\times\omega=1\,000\pi$, while the torque observer gains are the same as the velocity observer gains, except $\lambda_\tau=2$ Hz is added to the torque observer. From the computations that followed the stability analysis in Section 4, $(K_{s,\max})_T=7\,590$, and $(K_{s,\max})_{E2}=5\,331.46$. The sliding gain K_s is set smaller than the upper bounds. Finally, the velocity command is a ramp from zero to 1 000 rpm in 1.5 seconds as shown in Figs. 5 and 6. During the experiments, a disturbance torque provided by an electromagnetic

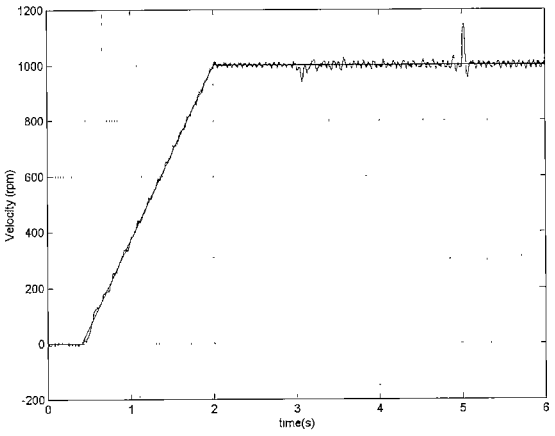

Fig. 5 Command velocity and actual motor velocity for the control system with the position and velocity observer

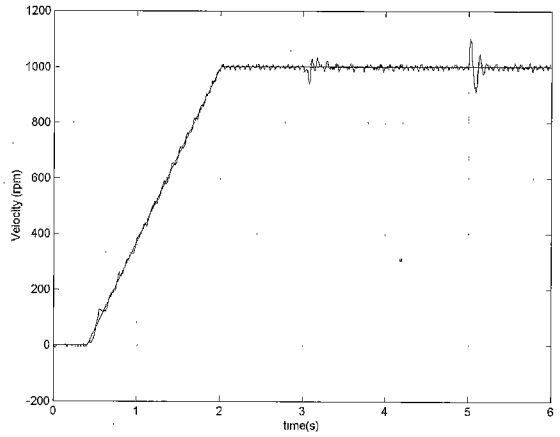

Fig. 6 Command velocity and actual motor velocity for the control system with the torque observer

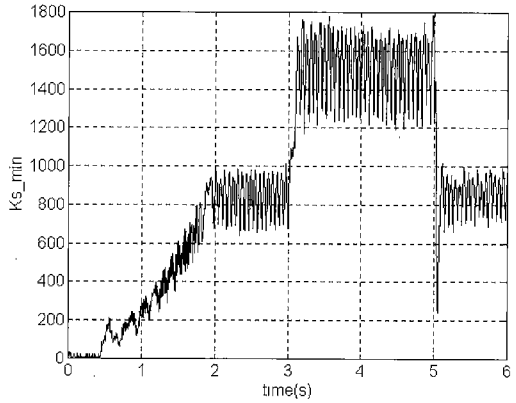

Fig. 7 The lower bound $K_{s,\min}$ for the control system with the position and velocity observer

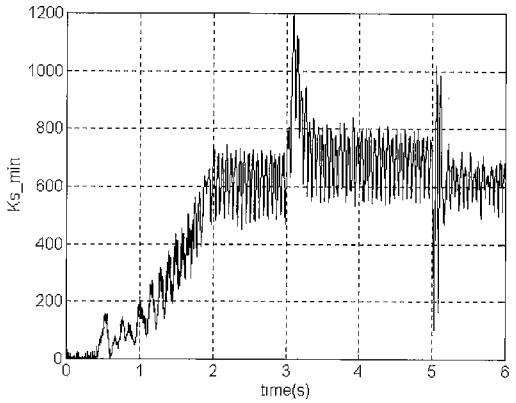

Fig. 8 The lower bound $K_{s,\min}$ for the control system with the torque observer

brake is applied to the motor between $t=3$ second and $t=5$ second. The lower bounds, $K_{s,\min}$, in Eq. (28) for both observers are shown in Figs. 7 and 8, respectively. By setting the sliding gain K_s larger than the lower bounds, the sliding surfaces, such as S_a, for both observers are around the sliding manifold, $\mathbf{S}=\mathbf{0}$ and $\dot{\mathbf{S}}=\mathbf{0}$, as shown in Figs. 9 and 10. Figures 5 and 6 indicate that, using both observers for sensorless speed control, the velocity of the motor tracks the command velocity accurately despite the disturbance torque. However, when the velocity observer is used

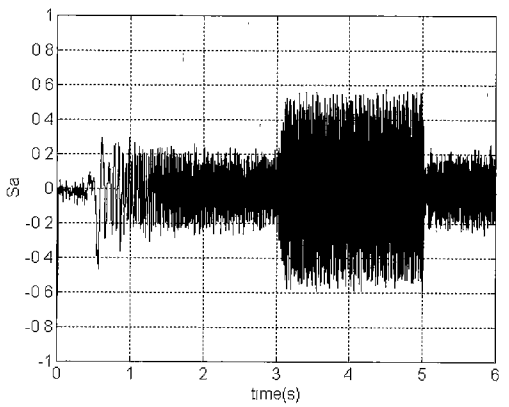

Fig. 9 The sliding surface S_a for the control system with the position and velocity observer

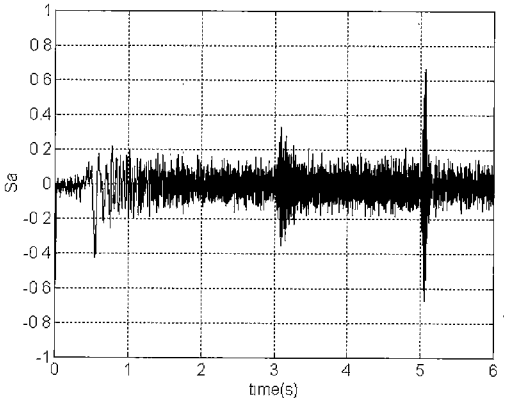

Fig. 10 The sliding surface S_a for the control system with the torque observer

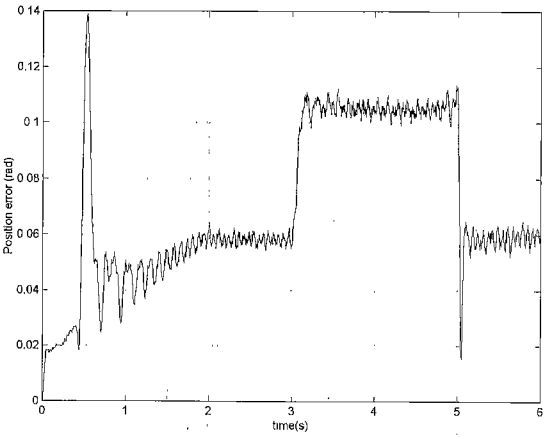

Fig. 11 Position estimation error for the control system with the position and velocity observer

alone, the estimation error of the rotor position is quite large if the external torque is present, as shown in Fig. 11. However, when the torque observer is also implemented, the estimation error of the rotor position is very small even if the external torque is not zero, as displayed in Fig. 12. The experimental results neatly confirm the analysis in Section 3.

6. Conclusion

Two nonlinear sliding observers are developed for speed-sensorless control of PMSM. One of the

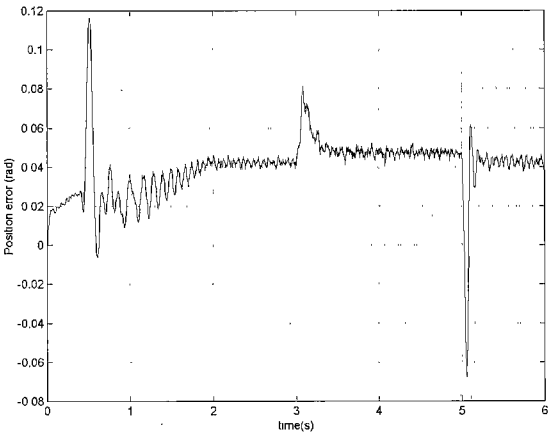

Fig. 12 Position estimation error for the control system with the torque observer

observers estimates the rotor position and velocity based on measurements of the current, while the other estimates the load torque in addition to the rotor position and velocity. From the observability analysis, the nonlinear systems are always observable except at $\omega=0$. The bounds of the sliding gain that guarantee the existence of the sliding manifold and the stability of the sliding observers are also outlined. It is found that if the sliding gain K_s is large enough to guarantee the existence of the sliding manifold, and also smaller than its upper bound for discrete-time stability, then the torque observer is locally stable at each speed except at $\omega=0$. Theoretical analyses and practical experiments both demonstrate that, using either observer for speed-sensorless control, the steady-state velocity error converges even when an external load torque is applied to the rotor. However, when an external load is present, the position estimation error of the control system with torque estimation and compensation is significantly smaller than that of the system without torque estimation and compensation. This study has demonstrated the feasibility of implementing a trajectory-tracking controller using the novel observer.

Acknowledgments

The authors would like to thank the National Science Council of the Republic of China for financially supporting this research under contract No. NSC89-2218-E-009-007.

References

(1) Kuo, B.C., Lin, W.C. and Goerke, U., Waveform Detection of Permanent-magnet Step Motors, Part I, Proceedings of Annual Symposium on Incremental Motion Control Systems and Devices, (1979), pp. 227-241.

(2) Kuo, B.C., Lin, W.C. and Goerke, U., Waveform Detection of Permanent-magnet Step Motors, Part II, Proceedings of Annual Symposium on Incremental Motion Control Systems and Devices, (1979), pp. 243-256.

(3) Wu, R. and Slemon, G.R., A Permanent Magnet Motor Drive without a Shaft Sensor, Conf. Rec. of the 1990 IEEE on Industry Applications Society Annual Meeting, (IAS '90), pp. 553-558.

(4) Jones, L.A. and Lang, J.H., A State Observer for the Permanent-Magnet Synchronous Motor, IEEE Trans. Ind. Electron., Vol. 36, No. 3 (1989), pp. 374-382.

(5) Low, T.-S., Lee, T.-H. and Chang, K.-T., A Nonlinear Speed Observer for Permanent-Magnet Synchronous Motors, IEEE Trans. Ind. Electron., Vol. 40, No. 3 (1993), pp. 307-316.

(6) Luenberger, D.G., An Introduction to Observers, IEEE Trans. Automat. Contr., Vol. AC-16, No. 6 (1971), pp. 594-602.

(7) Cho, K.-Y., Hong, S.-S., Oh, D.-S. and Youn, M.-J., Speed Control of Permanent Magnet Synchronous Motor Using Boundary Layer State Observer, Electronics Letters, 6th, Vol. 26, No. 25 (1990), pp. 2081-2082.

(8) Walcott, B.L. and Zak, S.H., Observation of Dynamical Systems in The Presence of Bounded Nonlinearities/Uncertainties, Proc. 25th IEEE CDC, (1986), pp. 961-966.

(9) Furuhashi, T., Sangwongwanish, S. and Okuma, S., A Position-and-Velocity Sensorless Control for Brushless DC Motors Using an Adaptive Sliding Mode Observer, IEEE Trans. Ind. Electron., Vol. 39, No. 2 (1992), pp. 89-95.

(10) Sheu, R., Sliding Observer-Based Variable Speed Control of Electrical Machines, Master Thesis, National Chiao-Tung University, (1994), Hsinchu City, Taiwan.

(11) Hu, J., Zhu, D., Li, Y. and Gao, J., Application of Sliding Observer to Sensorless Permanent Magnet Synchronous Motor Drive System, 25th Annual IEEE Conf. on Power Electronics Specialists Conference, (PESC '94 Record), Vol. 1 (1994), pp. 532-536.

(12) Utkin, V.I., Sliding Modes in Control and Optimization, (1992), pp. 207-210, Springer-Verlag, New York.

(13) Slotine, J.-J.E., Hedrick, J.K. and Misawa, E.A., On Sliding Observers for Nonlinear Systems, Journal of Dynamic Systems Measurement and Control, Vol. 109 (1987), pp. 245-252.

(14) Wang, H.R., Shaft Sensorless Speed Control of Permanent Magnet Synchronous Motors, Master Thesis, National Chiao-Tung University, (1996), Hsinchu City, Taiwan.

(15) Vidyasagar, M., Nonlinear System Analysis, (1993), Prentice-Hall.

(16) Middleton, R.H. and Goodwin, G.C., Digital Control and Estimation a Unified Approach, (1990), Prentice-Hall.